Tunability of intersubband absorption from 4.5 to 5.3 μm in a GaN/$Al_{0.2}Ga_{0.8}N$ superlattices grown by metalorganic chemical vapor deposition

N. Péré-Laperne, C. Bayram, L. Nguyen-Thê, R. McClintock, and M. Razeghi[a)]
Department of Electrical Engineering and Computer Science, Center for Quantum Devices, Northwestern University, Evanston, Illinois 60208, USA

(Received 10 August 2009; accepted 11 September 2009; published online 30 September 2009)

Intersubband (ISB) absorption at wavelengths as long as 5.3 μm is realized in GaN/$Al_{0.2}Ga_{0.8}N$ superlattices grown by metalorganic chemical vapor deposition. By employing low aluminum content $Al_{0.2}Ga_{0.8}N$ barriers and varying the well width from 2.6 to 5.1 nm, ISB absorption has been tuned from 4.5 to 5.3 μm. Theoretical ISB absorption and interband emission models are developed and compared to the experimental results. The effects of band offsets and the piezoelectric fields on these superlattices are investigated. © *2009 American Institute of Physics*. [doi:10.1063/1.3242027]

Recently III-Nitride semiconductors have become very attractive materials for the development of intersubband (ISB) devices. Being unipolar, ISB transitions allow for fast carrier relaxation process as well as wide-range tunability from near to far-infrared ($\lambda \sim 1-100$ μm). The large conduction band-offset between AlN and GaN ($\Delta E_c = 1.75$ eV) makes it possible to realize devices suitable for telecommunication wavelengths (1.3–1.6 μm).[1] In addition, the high electronic effective mass ($m^* \sim 0.2-0.3 \times m_0$) and the large longitudinal optical phonon energy (~90 meV) make this material interesting for high speed and high temperature ISB applications. Binary/binary (AlN/GaN) superlattices can be grown pseudomorphically and realized crack-free,[2] however the 2.4% lattice mismatch generates considerable spontaneous and piezoelectric polarization leading to multi-MV/cm electric fields, in conventional *c*-plane growth.[3]

Most III-Nitride ISB devices currently reported are based on binary AlN/GaN superlattices—in order to realize THz devices, the aluminum content in the $Al_xGa_{1-x}N$ barriers needs to be decreased to approximately 15%–20%.[4,5] Theoretical calculations to realize a terahertz emitter based on a cascade design working at room temperature have recently been demonstrated.[4–6] By changing the aluminum content in the $Al_xGa_{1-x}N$ barrier, the wavelength can be tuned to cover the infrared range all the way out to the terahertz. The use of ternary $Al_xGa_{1-x}N$ alloys as barriers decreases the internal electric field as there is less mismatch with respect to the GaN wells. This promotes better interface quality and thickness control over the AlGaN/GaN superlattice. III-Nitride ISB devices can be grown by metalorganic chemical vapor-phase epitaxy (MOCVD), however the few reports using MOCVD cover binary/binary superlattices absorbing in the shorter wavelength range from around 1.55 μm (Refs. 7 and 8) up to near-infrared ($\lambda = 2.4$ μm).[9] Today, most nitride based commercial optoelectronic devices are grown by MOCVD; thus, there is interest in using MOCVD to realize high-quality ISB devices at longer wavelengths from the infrared to terahertz wavelengths requiring alloy composition control of $Al_xGa_{1-x}N$ barriers.

In this work, we have used MOCVD to grow superlattices composed of GaN wells and $Al_{0.2}Ga_{0.8}N$ barriers in order to reach longer ISB wavelengths. The interband and ISB optical transitions of these superlattices are studied via photoluminescence (PL) and absorption measurements. The effects of well thickness and doping on the electronic transitions are simulated via theoretical analysis. We tuned ISB absorption from 4.5 to 5.3 μm in a GaN/$Al_{0.2}Ga_{0.8}N$ superlattices.

The material was grown in an AIXTRON 200/4-HT horizontal flow low-pressure MOCVD reactor. The superlattice layers were grown on a high-quality AlN template on double sided polished *c*-plane sapphire.[10] Trimethlyaluminum (TMAl) and trimethylgallium (TMGa) are used as the metalorganic precursors for Al and Ga, respectively; ammonia (NH_3) and hydrogen are used as the anion source and carrier gas, respectively. Silane (SiH_4) is used as the *n*-type dopant source. AlGaN layers were grown by simultaneously sending TMGa, TMAl, and ammonia; GaN:Si layers were grown by simultaneously sending TMGa, ammonia, and silane similar to our previous reports.[11] The active region consists of 50 periods of GaN wells with $Al_{0.2}Ga_{0.8}N$ barriers. In order to study the ISB transitions, several samples were grown with different well thicknesses (1.2, 2.6, 3.7, and 5.1 nm) employing a constant barrier thickness of 2.9 nm. All samples also have a 30 nm thick $Al_{0.2}Ga_{0.8}N$ capping layer. The same structures were also grown with doped wells ($Si: 1 \times 10^{18}$ cm^{-3}) to study the effects of doping.

In order to assess the structural properties of the superlattices, open detector omega/2theta (002) x-ray diffraction (XRD) scans are performed. Figure 1 represents the XRD plots for the four different well thicknesses. In Fig. 1, the narrowest peak located at 20.7° corresponds to sapphire substrate, the peak at 18.2° corresponds to AlN, and the zeroth order and first order superlattice peaks are also present. The average aluminum composition was calculated from the angular difference between the AlN peak and the zeroth order of the superlattice.[11,12] Once the average aluminum content was determined, we extracted the period of the superlattice from the spacing of satellite peaks.[13] The inset of Fig. 1 shows the calculated superlattice period as a function GaN growth time. By varying the GaN growth time (and keeping the AlGaN barrier thickness constant), a linear change in the GaN well width is observed, from the slope of which a GaN growth rate of 0.64 Å/s is extracted. The *y*-intercept then corresponds to the barrier thickness (which was held con-

a)Electronic mail: razeghi@eecs.northwestern.edu.

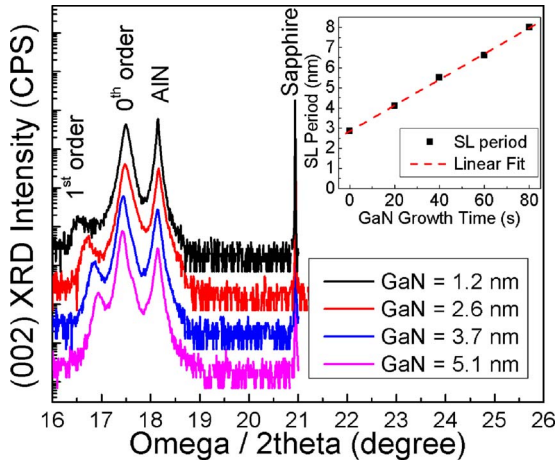

FIG. 1. (Color online) Omega/2theta (002) XRD of superlattices with four different well thicknesses: from top to bottom these are 1.2, 2.6, 3.7 nm and 5.1 nm GaN. Wells are Si doped to 1×10^{18} cm^{-3}. The barriers for all samples are 2.9 nm thick $Al_{0.2}Ga_{0.8}N$. Inset: superlattice period (from XRD analysis) as a function of well growth time is used to extract the GaN growth rate and determine the well thicknesses.

stant), evaluated to be 2.9 nm. By using this fixed barrier thickness together with the superlattice period and average composition, we are able to confirm the aluminum composition in the $Al_{0.20}Ga_{0.80}N$ barriers.

PL measurements were performed at room temperature using a frequency-doubled argon-ion laser emitting at 244 nm for excitation. The peak PL energy corresponds to the fundamental interband transition in the multiquantum-well structure. Figure 2 plots the PL intensity as a function of energy for 1.2, 2.6, 3.7, and 5.1 nm GaN well thicknesses (wells are Si doped 1×10^{18} cm^{-3}) and 2.9 nm $Al_{0.2}Ga_{0.8}N$ barrier (barriers are undoped). As expected, a redshift of PL emission is observed as the well thickness increases and the confined electron and hole states move toward the bottom of the wells. As the well width increases, the PL shifts until the sample with 5.1 nm thick well, it exhibits peak PL emission at 3.33 eV. Generally the bulk bandgap energy of GaN is taken to be 3.44 eV.[11] In the case of these $Al_{0.2}Ga_{0.8}N/GaN$ superlattices, the peak PL emission energy is below the bandgap energy due to the strain in the material.[14] In addition, the intensity of the PL emission decreases significantly with increasing well width; this behavior is also characteristic of strained material. In a strained

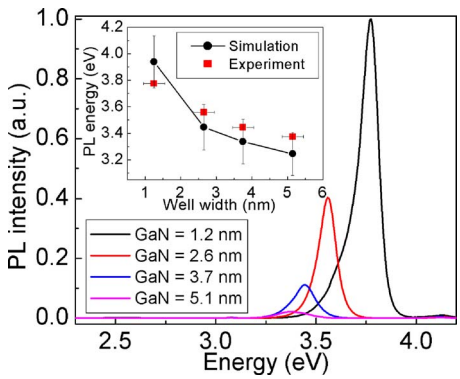

FIG. 2. (Color online) PL intensity as a function of energy for four different GaN well thicknesses: 1.2, 2.6, 3.7, and 5.1 nm—all with a constant 2.9 nm $Al_{0.2}Ga_{0.8}N$ barrier thickness. Superlattice consists of 50 periods where each well is Si doped to 1×10^{18} cm^{-3}. Inset: Comparison theory/experiment PL energy as a function of well width.

material, as the well thickness increases, the electron and hole wave functions are confined in the triangular part of the well due to the quantum confined Stark effect. As a consequence, the overlap between the two wave functions decreases resulting in decreased recombination efficiency and thus PL intensity. A Gaussian fit was performed on the PL emission peaks revealing a full width at half maximum (FWHM) for the 1.2, 2.6, 3.7, and 5.1 nm GaN well thicknesses of 111.5, 102.5, 127.5, and 172.5 meV, respectively. The FWHM tends to increase with well width except for a minor inconsistency for the first two FWHM values, likely due to inhomogeneous broadening from such thin well widths. These FWHM values are sufficiently narrow so as to imply good quality of the superlattice material grown.[15] The quality of the sample is also highlighted by the absence of any yellow peak in the PL emission, generally attributed to nitrogen vacancies or impurities.[16]

In order to interpret the PL results, we performed simulations of the electron and hole confinement in the conduction and valence bands. We solved the Schrödinger equation taking into account the band nonparabolicity using the energy-dependent effective-mass approach in the highly strained band profile. Parameters used for the simulation are the conduction and valence band offsets, the energy bandgap, and the strain. The strain is taken into account by applying an internal electric field to the wells and barriers. A rough estimation of the strain is achieved via linear interpolation of the constants used for binary/binary superlattices (SLs). The superlattice is a periodic structure, thus the internal electric fields applied to the GaN wells and $Al_{0.2}Ga_{0.8}N$ barriers depends on the polarization discontinuity, and the well and barrier thicknesses.[17,18] Polarization constants for the binary well and for the ternary barrier are taken from Ref. 1. The inset of Fig. 2 displays the experimental and theoretical PL energy as a function of the GaN well width. The interband simulations and PL experiments are in reasonably good agreement, however, a shift in wavelength between simulation and experiments is observed. This slight discrepancy of our experimental results with theory and with experimental results reported in Ref. 15 can be accounted for by uncertainties in the layer thicknesses (error bars one monolayer) and strain in the AlGaN/GaN structure (error 5%). Indeed, the simulation assumes the structure is fully strained with respect to the barrier material ($Al_{0.2}Ga_{0.8}N$) whereas in the real structure there may be partial relaxation occurring at the $Al_{0.2}Ga_{0.8}N$ on GaN interfaces, interfacial roughness, or incomplete relaxation at the AlGaN/AlN template interface. Further investigations, like XRD reciprocal space mapping may be able to provide a better estimate of the true strain.

We also performed the same PL experiments for the undoped samples. These samples have the same superlattice structure as the doped samples, however there is a slight redshift in PL emission with respect to the doped samples. This shift to lower energy for the undoped samples can be attributed to the partial carrier screening of the internal electric field.[19]

ISB absorption measurements were realized using a Bruker IFS 66V vacuum Fourier transform infrared spectrometer, with an internal blackbody source, and a cryogenic mercury-cadmium-telluride detector. Samples were cut into 4 mm long bars and 45° angle facets were polished on both sides in order to form a multipass waveguide. A wire-grid

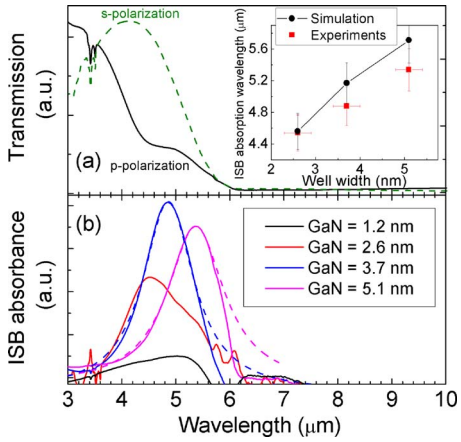

FIG. 3. (Color online) (a) Solid line is the *p*-polarization transmission for 2.6 nm well width and 2.9 nm barrier with, wells are Si doped to 1×10^{18} cm^{-3}, the dashed line corresponds to *s*-polarization transmission for the same sample. Inset: ISB absorption wavelength as a function of well width—experimental results (squares) and simulation (circles) for a fully strained structure. (b) From left to right, ISB absorbance for 1.2 nm (black), 2.6 nm (red), 3.7 nm (blue), and 5.1 nm (magenta) well widths. Lorentzian fits are shown (dashed lines) for the 3.7 and 5.1 nm well widths.

polarizer was inserted into the beam-path just before the sample to select either *p*- or *s*-polarization for the incident light. Figure 3(a) presents both *p*-polarization (solid line) and *s*-polarization (dashed line) raw transmission data for the sample with doped 2.6 nm wells and 2.9 nm barriers. For both polarizations, we observe 100% absorption above $\lambda = 6.1$ μm—this is attributed to absorption in the sapphire substrate. This absorption represents a significant limiting factor in the development of longer wavelength devices. An absorption edge is also observed in the *p*-polarization at a wavelength of 4.5 μm whereas no corresponding absorption is observed for *s*-polarization verifying this feature as ISB absorption. For the four well widths, the negative logarithm of the ratio of the two spectra (*p*-polarization and *s*-polarization) normalized by the open beam are plotted in Fig. 3(b), this corresponds to the ISB absorbance. For the well width of 1.2 nm, no clear absorption feature is observed; this agrees with theory as only one bound state is present in this well, and thus ISB transition should occur between one bound state and the continuum of states above the barriers. Concerning the three remaining well widths, the ISB absorbance peaks are at 4.5, 4.9, and 5.3 μm for the 2.6, 3.7, and 5.1 nm well widths, respectively. The increasing well width redshifts the ISB absorption peak as the two first confined states of the well become closer in energy. For the 2.6 nm thick well we observe a broader absorption peak compared to the two wider wells (3.7 and 5.1 nm). For the 2.6 nm well width, some oscillations appear around 6 μm in the absorbance, these are attributed to the normalization with *s*-polarized spectra close to the sapphire cut-off. For each of the two wider wells we observe one prominent absorption feature that can be fitted with Lorentzian functions (dashed lines), characteristic of ISB transitions. Lorentzian functions do not perfectly fit the experimental curves around 6 μm due to the normalization. Furthermore, the decrease of ISB absorption intensity as the well width increases is explained by the decrease of quantum confinement for the second subband compared to the fundamental state reducing the optical dipole matrix element.

The ISB absorption wavelength as a function of well width was simulated; a comparison with the experimental data is shown in the inset of Fig. 3(a). A very good fit is obtained for the thinnest well (2.6 nm), but the discrepancy increases as the well width increases. It may be explained by the variation behavior of the background and then, the normalization (error 5%). Plus, this discrepancy is attributed to uncertainties in internal electric field and conduction band offset as the two subbands are located in the triangular part of the well for thicker wells (error 5%). Further studies of these two parameters are required to minimize this discrepancy.

In summary, we have studied $Al_{0.2}Ga_{0.8}N/GaN$ superlattices grown by MOCVD with various well thicknesses via XRD, PL, and polarization dependent ISB absorption measurements. A theoretical model was developed taking into account strain in binary/ternary superlattices to correlate with both experimental interband emission and ISB absorption results. Ultimately we demonstrate tunability of ISB absorption from 4.5 to 5.3 μm in a $GaN/Al_{0.2}Ga_{0.8}N$ superlattice. This demonstration is an important step toward employing GaN/AlGaN SLs in longer wavelength ISB devices.

The authors would like to thank Dr. D. Silversmith of the AFOSR, Dr. H. Temkin, and Dr. M. Rosker of DARPA, and Dr. J. Zavada of ARO for their support and encouragement, and Dr. Matthew Grayson for critical reading of this manuscript.

[1] I. Vurgaftman and J. R. Meyer, J. Appl. Phys. **89**, 5815 (2001).
[2] A. D. Bykhovski, B. L. Gelmont, and M. S. Shur, J. Appl. Phys. **81**, 6332 (1997).
[3] N. Suzuki, N. Iizuka, and K. Kaneko, Jpn. J. Appl. Phys., Part 1 **42**, 132 (2003).
[4] V. D. Jovanovic, D. Indjin, Z. Ikonic, and P. Harrison, Appl. Phys. Lett. **84**, 2995 (2004).
[5] G. Sun and R. A. Soref, Microelectron. J. **36**, 450 (2005).
[6] N. Vukmirovic, V. D. Jovanovic, D. Indjin, Z. Ikonic, P. Harrison, and V. Milanovic, J. Appl. Phys. **97**, 103106 (2005).
[7] E. Baumann, F. R. Giorgetta, D. Hofstetter, S. Golka, W. Scherenk, G. Strasser, L. Kirste, S. Nicolay, E. Feltin, J. F. Carlin, and N. Grandjean, Appl. Phys. Lett. **89**, 041106 (2006).
[8] S. Nicolay, E. Feltin, J. F. Carlin, N. Grandjean, L. Nevou, F. H. Julien, M. Schmidbauer, T. Remmele, and M. Albrecht, Appl. Phys. Lett. **91**, 061927 (2007).
[9] I. Waki, C. Kumtornkittikul, Y. Shimogaki, and Y. Nakano, Appl. Phys. Lett. **82**, 4465 (2003); **84**, 3703 (2004).
[10] C. Bayram, J. L. Pau, R. McClintock, and M. Razeghi, J. Appl. Phys. **104**, 083512 (2008).
[11] C. Bayram, N. Péré-laperne, R. McClintock, B. Fain, and M. Razeghi, Appl. Phys. Lett. **94**, 121902 (2009).
[12] S. Zhou, M. F. Wu, S. D. Yao, B. S. Zhang, and H. Yang, Superlattices Microstruct. **40**, 137 (2006).
[13] M. A. Moram and M. E. Vickers, Rep. Prog. Phys. **72**, 036502 (2009).
[14] M. Tchernycheva, L. Nevou, L. Doyennette, F. H. Julien, E. Warde, F. Guillot, E. Monroy, E. Bellet-Amalric, T. Remmele, and M. Albrecht, Phys. Rev. B **73**, 125347 (2006).
[15] N. Grandjean, J. Massies, and M. Leroux, Appl. Phys. Lett. **74**, 2361 (1999).
[16] L. Polenta, A. Castaldini, and A. Cavallini, J. Appl. Phys. **102**, 063702 (2007).
[17] D. Vanderbilt and R. D. King-Smith, Phys. Rev. B **48**, 4442 (1993).
[18] M. Leroux, N. Grandjean, J. Massies, B. Gil, P. Lefebvre, and P. Bigenwald, Phys. Rev. B **60**, 1496 (1999).
[19] A. Helman, M. Tchernycheva, A. Lusson, E. Warde, F. H. Julien, Kh. Moumanis, G. Fishman, E. Monroy, B. Daudin, D. Le Si Dang, E. Bellet-Amalric, and D. Jalabert, Appl. Phys. Lett. **83**, 5196 (2003).